Hindawi Publishing Corporation
Journal of Nanomaterials
Volume 2015, Article ID 104193, 10 pages
http://dx.doi.org/10.1155/2015/104193

Research Article

Influence of Anodic Oxidation Parameters of TiO_2 Nanotube Arrays on Morphology and Photocatalytic Performance

Xiaoyu Zhao, Yuxiang Zhu, Yanfei Wang, Liang Zhu, Libin Yang, and Zuoliang Sha

Tianjin Key Laboratory of Marine Resources and Chemistry, College of Chemical Engineering and Materials Science, Tianjin University of Science and Technology, No. 29, 13th Avenue, TEDA, Tianjin 300457, China

Correspondence should be addressed to Xiaoyu Zhao; xyz@tust.edu.cn and Zuoliang Sha; zsha@tust.edu.cn

Received 18 June 2015; Accepted 9 August 2015

Academic Editor: Cunming Liu

Titanium dioxide nanotube arrays (TNTAs) were fabricated by electrochemical anodization of Ti foils. The effects of electrolyte, applied voltage, duration of anodic oxidation to morphology, and photocatalytic performance of TNTAs were investigated. TNTAs formed in electrolyte of glycol and DMSO tend to grow along radial direction with flimsy tube wall and weak adhesion on Ti substrate. Those in glycerol, however, easily achieve balance between growth rate and corrosion rate, form orderly arranged array of nanotubes with uniform diameter, moderate length, and strong adhesiveness with substrates then. Although the photocatalytic activity of Rh B degradation on TNTAs prepared in glycol and DMSO is higher than those prepared in glycerol, their convenience of recycling and recovery shows the opposite. The optimality condition of anodic oxidation for TNTAs with good morphology and photocatalytic performance was present, which may have potential application in the synthesis of composite nanoarrays.

1. Introduction

Ever since carbon nanotubes were discovered by *Iijima*, nanomaterials with tube structure have attracted widespread attention from different research area due to its unique geometric structure and advanced physicochemical properties. As one of those nanotube materials, titanium dioxide nanotube arrays (TNTAs) have been applied to many fields, such as photocatalytic hydrogen generation, photovoltaic cells, degradation of organic contaminants, and gas sensor, because of their excellent specific surface area, high adsorption capacity, and less agglomeration [1–13]. Recently, multiple methods of preparation on TNTAs have been proposed: hydrothermal synthesis method, template method, and electrochemical anodic oxidation [14–16]. TNTAs prepared by the first two approaches are dispersed powders, which cannot adhere to the substrate firmly and are hard to be recycled. On the other hand, TNTAs prepared by electrochemical anodic oxidation adhered to the Ti substrate firmly with highly ordered array structures. Furthermore, the morphology of TNTAs can be controlled by adjusting experimental parameters.

Large-scale TNTAs composed of many single and well-arranged TiO_2 nanotubes were prepared by potentiostatic anodic oxidation of Ti foils with 0.5 wt% HF electrolyte, as Gong et al. reported at 2001 [17]. After that, the anodic oxidation method of preparing TNTAs has been studied by many researchers; it can be divided into three stages according to length of nanotube or electrolyte composition. The first TNTA generation is produced in strong acid electrolyte containing HF with pH lower than 3; its length is 500 nm below the general length [18]. The second TNTA generation is prepared at weak acid fluoride aqueous electrolyte with pH between 3 and 6; its length can reach 6.4 μm [14]. The last TNTAs generation, revolutionarily, uses organic instead of aqueous solvent as electrolyte [14, 16, 19–21]. Macak et al. prepared TNTAs by anodic oxidation and used glycol containing 0.5 wt% NH_4F as electrolyte firstly, whose length reaches 7 μm. However, the disadvantages are so fateful that they cannot be ignored: the length of tubes and specific surface area of TNTAs are distributed inhomogeneously. Besides, those tubes hardly adhere on substrates firmly [22–26]. Since then, scientists tried to design and achieve various geometrical

structures, such as stacking-type tube, chain-type tube, Bamboo-type tube, branched-type tube, and 3D complicated structure, by controlling the potential and electrolyte of anodic oxidation [27–31]. Nevertheless, to capitalize on TNTAs as photocatalysts is still a major challenge; that is, efficiencies of photoinduced processes are very low. This occurs because photocatalytic reaction rates are not fast enough to compete with the charge-recombination (electron-hole recombination). To address these problems, scientists focus on decorating TNTAs with noble metals or other nanomaterials with synergistic effect [14, 32–37]. As the starting point, the optimum condition of suitable TNTAs for decorating with materials should be investigated.

In this paper, by employing glycol, DMSO, glycerol, and $(NH_4)_2SO_4$ as main electrolytes, respectively, the effects of electrolyte and applied electric potentials on morphology of TNTAs were explored. Furthermore, photocatalytic degradation of Rhodamine B (Rh B) on TNTAs prepared from different electrolytes was compared under UV irradiation. In addition, the optimum condition TNTAs fabrication for nanoparticle deposition was discussed.

2. Experimental

2.1. Chemicals. Water used was ion-exchanged at first, distilled, and then ion-exchanged again by ultrapure water system. The purified water exhibited the ionic resistivity of 18 MΩ cm in the water system. Other chemicals were of analytical grade and were used as received.

2.2. Preparation of TNTAs. Well-ordered TNTAs were fabricated by electrochemical anodization in a two-electrode cell which consisted of Ti foils as working electrode and a Pt foil as counter electrode. Prior to the anodization, Ti foils (2.0 × 5.0 cm^2) were ultrasonically cleaned in acetone, methanol, and ethanol for 10 min followed, respectively, by deionized water rinse.

All electrolytes were prepared as a certain proportion, stirred by magnetic stirring until complete dissolve is achieved. In this study, four typical electrolytes were employed: 0.1 M NH_4F and 0.5 M $(NH_4)_2SO_4$ mixture solution; mixture solution composed of 98% dimethyl sulfoxide (DMSO) and 2% HF in volume; NH_4F with concentration of 0.075 M dissolved in mixture solvent which is composed of H_2O (3%, v/v) and glycol (97%, v/v); NH_4F with concentration of 0.27 M dissolve in mixture solvent composed of water and glycerol with ratio of 1 : 1 by volume.

The equipment of anodic oxidation is illuminated as Figure 1; the anode and cathode electrodes were pretreated titanium foil and Pt, respectively. The distance between two electrodes was 2 cm. Applied voltage started from 0 V to a certain voltage with rate of 250 mV/s and then maintained a certain time.

The Ti foil was drawn out from electrolyte after the anodic oxidation process and then washed by deionized water in order to remove adsorbed electrolyte on the surface, followed by six times of ultrasonic cleaning every 10 seconds. Then the resulting TNTAs were dried under room temperature before next process.

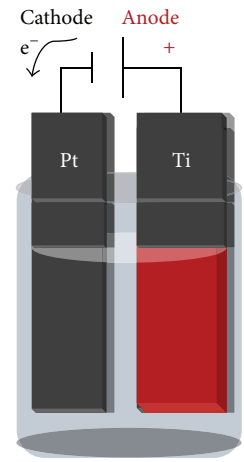

Figure 1: Schematic illustration of an electrochemical anodic oxidation cell.

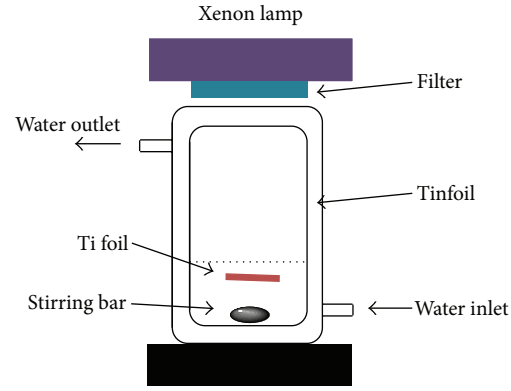

Figure 2: Schematic illustration of the photocatalytic reactor.

The dried TNTAs were put into muffle furnace which was firstly heated up to 200°C with 3°C/min and kept for 30 min, then was heated up to 450°C with 2°C/min and kept for 3 h, and was naturally cooled to room temperature at last.

2.3. Characterization. XRD patterns were acquired on a Bruker Axs D2 PHASER diffractometer with a Cu Kα X-ray source. Scan range located from 21° to 80°. The morphology of the obtained samples was characterized by a field emission scanning electron microscope (FESEM, Hitachi S-4800). The ultraviolet-visible (UV-Vis) spectra analysis was also performed on a Shimadzu UV-3600 spectrophotometer equipped with an integrating sphere using $BaSO_4$ as the reference.

2.4. Photocatalytic Activity. As shown in Figure 2, the photocatalytic activities were evaluated based upon the removal of Rh B solution with an initial concentration of 5 mg·L^{-1} in a glass reactor with a water jacket to control the reaction temperature. For comparison, the photocatalytic activities of TNTAs obtained from different electrolytes were also studied. A 300 W xenon lamp with a 365 nm filter was employed as the simulated ultraviolet source. The distance between the xenon

lamp and the TNTAs film was 13 cm. Prior to photocatalytic degradation, the samples were immersed in 20 mL Rh B aqueous solution with magnetic stirring in the dark for 1 h to establish an adsorption-desorption equilibrium at constant room temperature. After UV irradiation started, the solution periodically taken from the reactor was analyzed with a UV-Vis spectrophotometer. The analytical wavelength selected for optical absorbance measurement was 560 nm.

Based on Lambert-Beer law, there is a proportional relationship between concentration of absorbing material and absorbance, as shown in the following equation:

$$A = \lg\left(\frac{1}{T}\right) = Kbc, \quad (1)$$

in which A indicates absorbance; T indicates transmittance; K indicates characteristic constant; b indicates thickness of absorption layer with unit of cm; c indicates concentration of absorbance with unit of $mg{\cdot}L^{-1}$. Therefore, change of absorbance reflects change of concentration of Rh B solution. Normalized concentration ratio of Rh B solution is close to normalized maximum absorbance ratio (A/A_0); as a result, C/C_0 can be replaced by value of A/A_0.

3. Results and Discussion

3.1. Morphology of TNTAs. We present the SEM results of TNTAs obtained from four different electrolytes. Figures 3(a) and 3(b) show TNTAs prepared by anodic oxidation employing NH_4F and $(NH_4)_2SO_4$ mixed aqueous solution as electrolyte under constant applied voltage of 20 V for 2 h. Those nanotubes show irregular arrangement with nonuniform diameter of about 80 nm.

Figures 3(c) and 3(d) show top and cross-sectional views of TNTAs prepared by anodic oxidation with DMSO and HF mixed solution as electrolyte under constant applied voltage of 35 V for 2 h. Although the length of tubes reached 4 μm, it is clear that the tube entrance collapses seriously, coupled with broken surface which may be caused by relatively high voltage.

Figures 3(e)–3(h) show top, bottom, cross-sectional, and truncation views of TNTAs prepared by anodic oxidation employing NH_4F and glycol mixed aqueous solution as electrolyte under constant applied voltage of 20 V for 2 h. Nanotubes obtained under this condition are more complicated. Their surface shows weed-like features and bottom shows typical hexagon, while the walls are so smooth. The cross-link between those walls obviously decreased when compared to other TNTAs. Those nanotubes easily fall off from Ti substrate although the length of them reaches about 33 μm. Nanotube entrance collapse and broken surface may be attributed to the inhomogeneity of the tube structure. Fast growth rate along the tube leads to thinness of tube walls. As a result, those tubes cannot sustain the weight and thermal stress of themselves during the drying process.

Figures 3(i) and 3(j) show top and cross-sectional views of TNTAs prepared by anodic oxidation by employing NH_4F and glycerol mixed aqueous solution as electrolyte under applied constant voltage of 20 V for 2 h. The diameter of these tubes is uniform with 100 nm for inner and 117 nm for outer. The length is about 1 μm. Ripples on the tube walls can be seen, which indicates that the participation of water into electrolyte is necessary for oxidation corrosion of Ti foils. The corrosion rate of Ti foils and growth rate of TiO_2 are affected by the content of water. The formation of nanotubes with corrugated tube wall needs relative high content of water. These tubes adhere on the substrate firmly, which performs good stability of geometric structure and conveniences of recycling.

Then it can be concluded that NH_4F and glycerol mixed aqueous solution is the preferential electrolyte among those four kinds of electrolytes in this study. Therefore, based on this electrolyte system, other operating parameters including applied voltage and duration of anodic oxidation have been studied.

Figure 4 shows top view of TNTAs prepared at condition of (a) (20 V, 2 h), (b) (20 V, 6 h), (c) (25 V, 2 h), (d) (25 V, 6 h), (e) (30 V, 2 h), and (f) (30 V, 6 h), respectively. With the increase of applied voltage from 20 V, the diameter of nanotubes remains unaffected; however, the tube entrance becomes uniform and arrangement of nanotubes decreases seriously. Also the shape of tubes and thinness of tube walls tend to be inhomogeneous with increase of voltage.

As is seen in Figure 4, with the duration of anodic oxidation from 2 h to 6 h, tubular structure is severely damaged. The possible explanation might be that two dynamic processes contributed to the growth of tube on radial direction: anodic oxidation of Ti substrate to form fresh TNTAs and dissolution of tubes on the top part. There is an optimum duration of oxidation which is defined to be the equilibrium of those two dynamic processes. Longer time may unbalance the equilibrium, which forces the growth of tubes to be affected by diffusion, gravity, viscosity, and so forth.

3.2. Growth Mechanism of TNTAs. The key process of electrochemical oxidation can be explained as follows: firstly, oxides were formed on metal surface under the influence of interaction of oxygen ions or hydroxide ions. After that, those anions cross through oxidation layer and migrate to metal/oxide interface to react with metal. Secondly, under the effects of external electric field, tetravalent titanium ion (Ti^{4+}) migrates from metal/oxide surface to oxide/electrolyte surface. Electric field assisted dissolve will be the third step: under effect of external electric field, Ti–O bond undergoes polarization and is weakened, accelerating the dissolution of the metal cations. After Ti^{4+} dissolved into electrolyte, free oxygen anions migrate to metal/oxide intersurface and then interact with metal as mentioned at the first step. Lastly, chemical dissolve of metal or oxide occurs in acidic electrolyte. Chemical dissolve of TiO_2 in fluoride ion electrolyte plays a crucial role on formation process of nanotubes. Schematic diagram of ions migration was shown in Figure 5.

At the beginning of anodic oxidation, the initial oxidation layer was formed by interaction of Ti^{4+} ions on surface and O^{2-} ions in electrolyte, which can also be seen as distributed homogenously on the surface. The anodic oxidation of metal to form hydrogen ions and electrons is shown in

$$Ti + 2H_2O \longrightarrow TiO_2 + 4H^+ + 4e^- \quad (2)$$

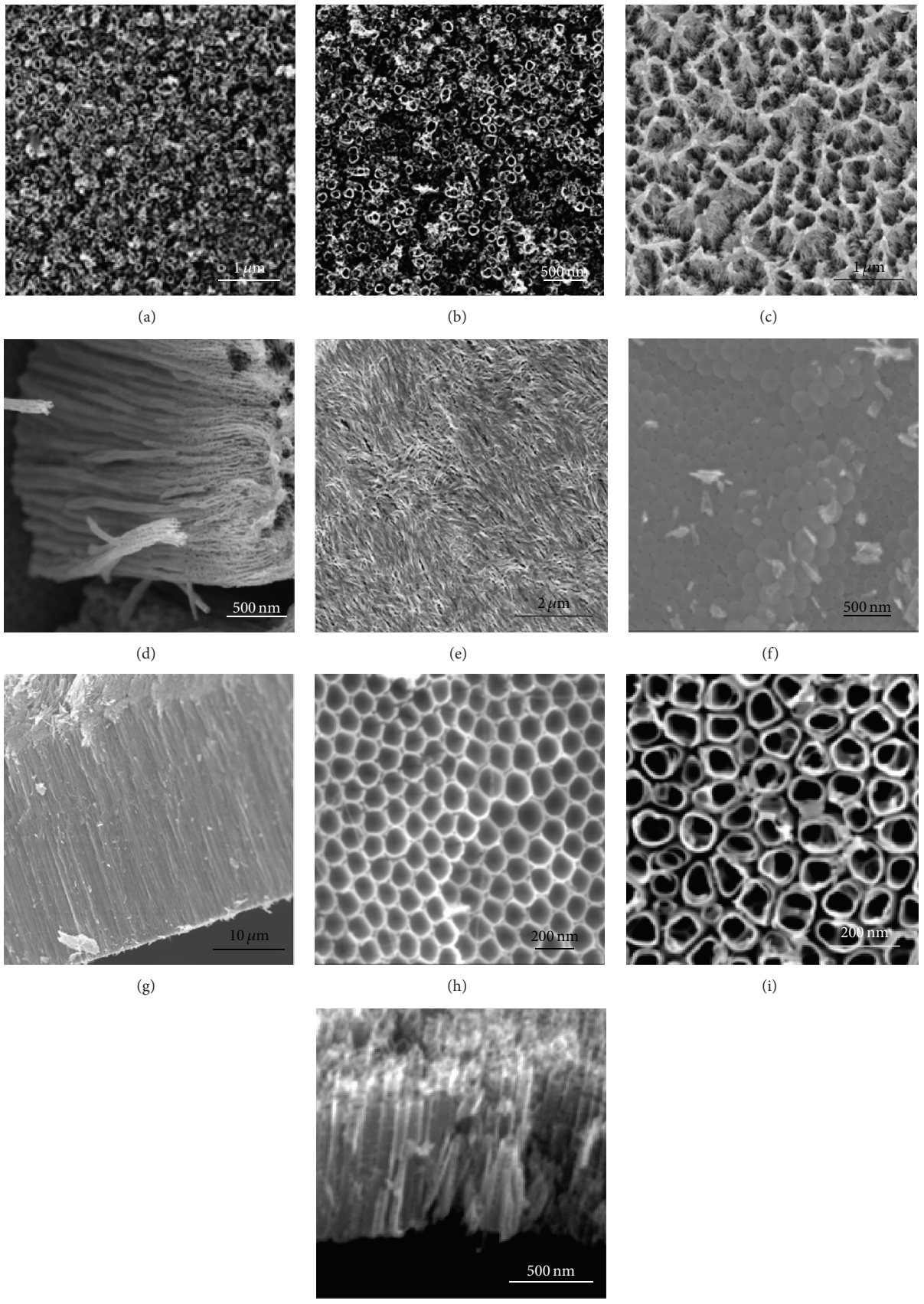

Figure 3: FE-SEM images of TNTAs fabricated by different solutions.

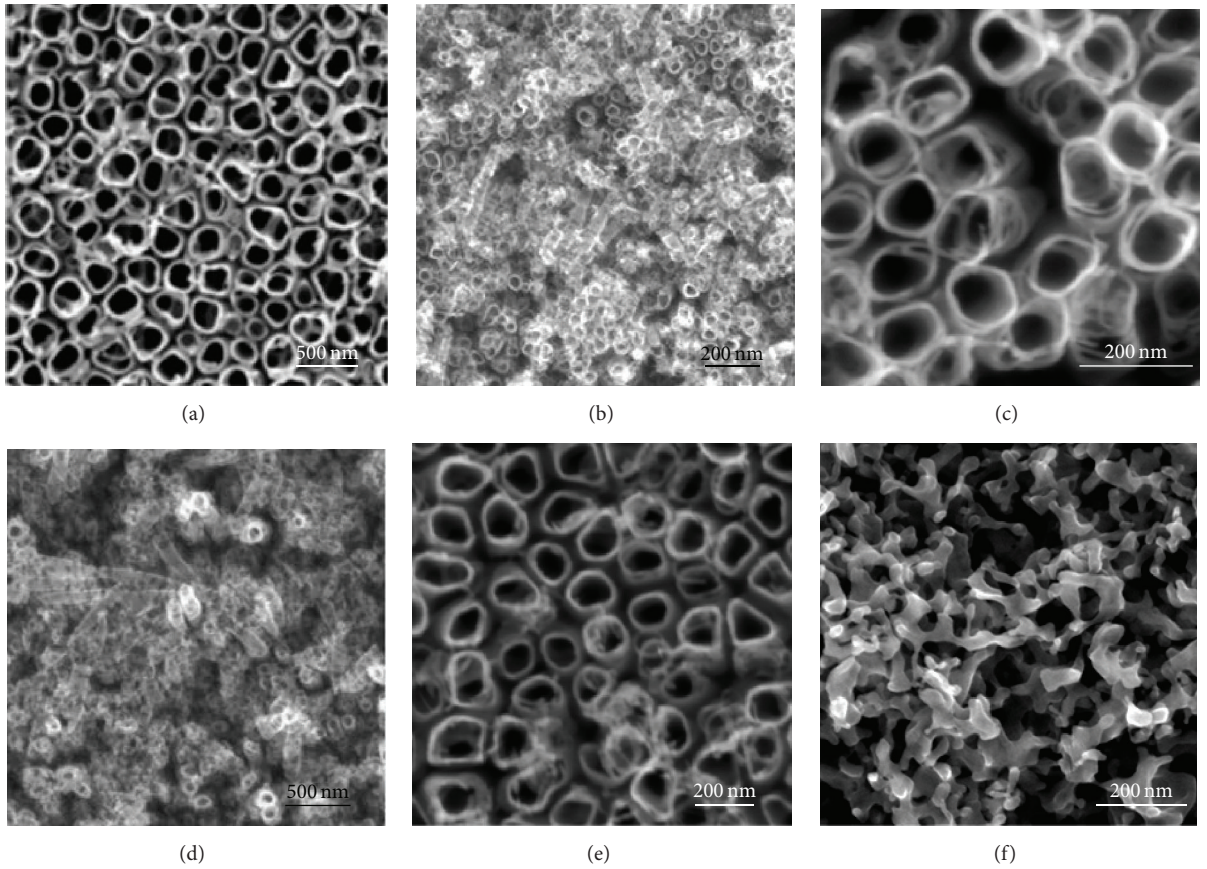

Figure 4: FE-SEM images of TNTAs fabricated by glycerol based solutions under different voltage and anodic oxidation time.

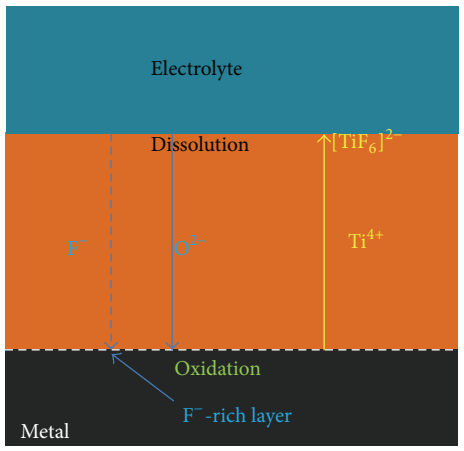

Figure 5: Schematic drawing showing field-aided transport of mobile ions through the oxide layers in the presence of fluoride ions.

Hydrogen generated at cathode is as follows:

$$8H^+ + 8e^- \longrightarrow 4H_2 \quad (3)$$

The total oxidation process can be given by

$$Ti + 2H_2O \longrightarrow TiO_2 + 2H_2 \quad (4)$$

Fluorine ions may attack water molecule and oxidation layer; in other words, ions migrating on anode layer under external electric field could react with Ti^{4+} anions:

$$TiO_2 + 6F^- + 4H^+ \longrightarrow [TiF_6]^{2-} + 2H_2O \quad (5)$$

$$Ti(OH)_4 + 6F^- \longrightarrow [TiF_6]^{2-} + 4OH^- \quad (6)$$

$$Ti^{4+} + 6F^- \longrightarrow [TiF_6]^{2-} \quad (7)$$

As shown in Figure 6(a), a thin layer formed on the titanium surface with start of anodic oxidation. Since partial dissolve of oxide may make the barrier layer at the bottom of concave thin, as can be seen in Figure 6(b), the electric field intensity at those remaining barrier layers increased resulting in further growth of pore. As shown in Figure 6(c), pores of tube appear relatively narrow since the field associated dissolve has no influence on formation of pores. However, the electric field distribution at bottom surface of the pore may broaden diameter of tubes as well as deepen cracks, which causes pores of nanotubes formed like a scallop shape. Since the bond energy of Ti–O is rather high, for TiO_2, it can be predicted reasonably that pores only can be formed on those thin walls, which can be contributed by relatively low ionic mobility and rather high chemical solubility of oxide in electrolyte. The electric field intensity at protruding metal area will increase with the growth of pores, which may enhance

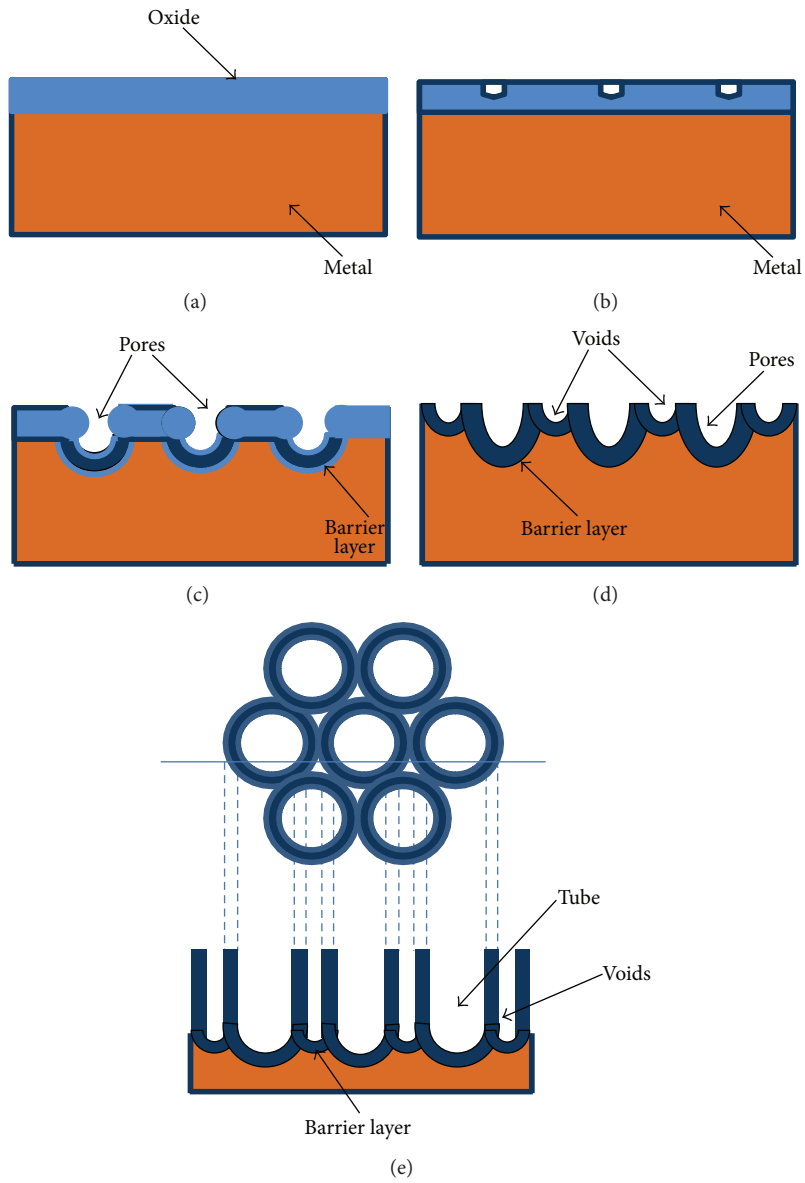

Figure 6: Schematic diagram of nanotube evolution at constant anodization voltage: (a) oxide layer formation, (b) pit formation on the oxide layer, (c) growth of the pit into scallop shaped pores, (d) the metallic region between the pores undergoing oxidation and field assisted dissolution, and (e) fully developed nanotubes with a corresponding top view.

the field associated growth of oxide and dissolution of oxide. Meanwhile, uniformly distributed pores and voids between pores formed in Figure 6(d). Subsequently, voids and pores grow together under equilibrium condition. The length will increase until the balance is achieved between electrochemical corrosion rate and chemical dissolve rate on the top surface of nanotubes. Thereafter, the length of nanotubes is finally achieved by given anodic oxidation time, concentration of electrolyte, and anodic oxidation voltage.

3.3. XRD Characterization. As seen in Figure 7, XRD characterization of TNTAs obtained in four different electrolytes has been presented. Five diffraction peaks at 25.2°, 37.8°, 48.1°, 53.9°, and 55.1° indicate crystal phase of anatase at (101), (004), (200), (105), and (211), respectively, according to JCPDS number 21-1272. It is obvious that anatase TNTAs can be obtained by annealing at 450°C. Peak intensities of crystal plane (101) for TNTAs prepared at glycerol aqueous electrolyte and NH_4F and $(NH_4)_2SO_4$ mixed aqueous electrolyte appear lower than those prepared at glycol electrolyte and DMSO electrolyte. This can be explained by the fact that ratio of TiO_2 is deeply influenced by length of nanotube, which is in accordance with SEM results. Besides, XRD characterization of Ti substrate and TNTAs fabricated in NH_4F and glycerol mixed aqueous solution were presented, respectively, before and after TNTAs are annealed (Figure 8). It can be seen that after anodization process TNTAs are amorphous and upon annealing they become anatase.

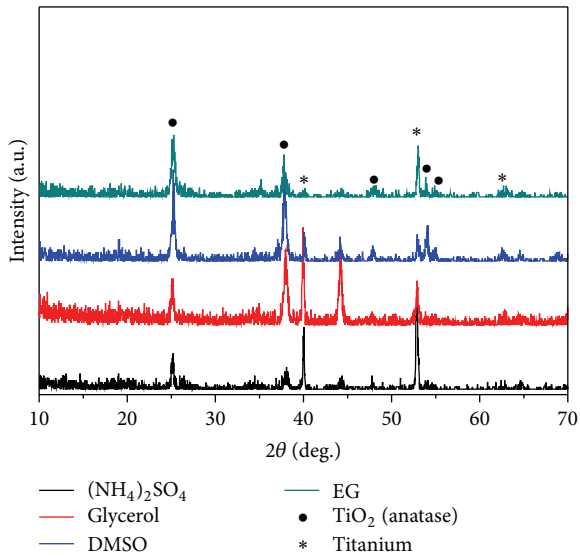

Figure 7: XRD patterns of TNTAs fabricated by different solutions.

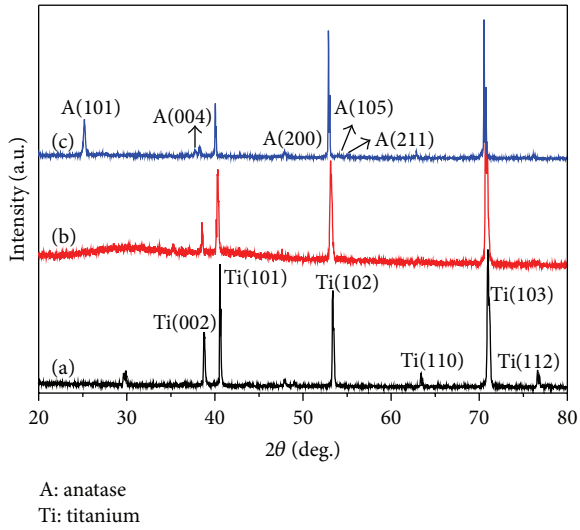

Figure 8: XRD patterns of TNTAs fabricated in NH_4F and glycerol mixed aqueous solution ((a) Ti substrate; (b) before annealing; (c) after annealing).

3.4. UV-Vis Diffuse Reflection Spectroscopy. The optical properties of TNTAs prepared at different electrolytes were studied by UV-Vis diffuse reflection spectroscopy, as shown in Figure 9. Light response range of all TNTAs reported here is localized in ultraviolet range. However, TNTAs prepared by glycerol electrolyte, in spite of its disadvantage at length of nanotube, show highest intensity of light adsorption at tail. This may benefit from the uniformity of nanotube arrangement and less collapse on nanotube entrance. For those TNTAs obtained by other electrolytes, although length of nanotube may have its edge, collapse on nanotube entrance or structures with weed-like features and disordered orientation result in the fact that the obstacle of incident light could not pass into passageway of nanotubes, eventually.

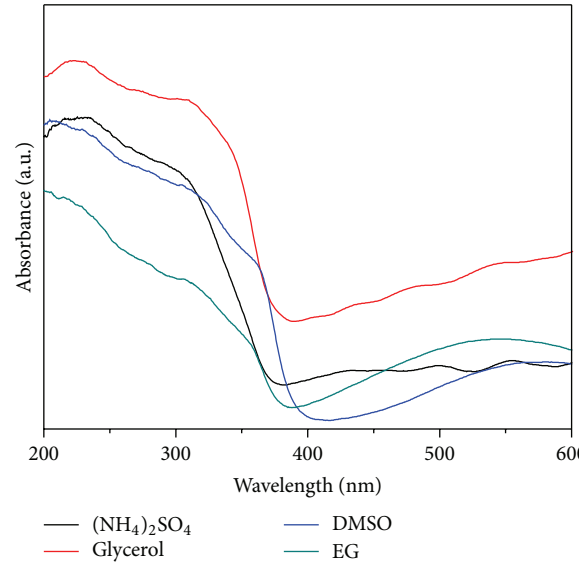

Figure 9: UV-Vis spectra TNTAs made in different solutions.

3.5. Photocatalytic Activity on Degradation of Rh B. TNTAs are one of the most active materials for degradation of contaminants especially for organic pollutants. This may be contributed by the proximity between conduction band edge of TNTAs and redox potentials of the surroundings such as water. Rh B, as one of the most water pollutants, is stable and carcinogenic [38]. The photocatalytic activities of TNTAs fabricated in four different electrolytes were investigated by degrading Rh B.

The variation of C/C_0 with illumination time is shown in Figure 10(a), in which C_0 indicates the initial concentration after the adsorption equilibrium is established, while C indicates concentration of reaction solution extracted out every 30 minutes. It can be seen from blank curve of Figure 10(a) that the Rh B molecule is extremely stable under UV irradiation without the presence of catalysts. Also, after irradiation of 210 minutes by UV, Rh B shows no evidence of decomposition, which indicates impossibility of self-degradation. The degradation efficiencies of TNTAs prepared in electrolytes of glycol, DMSO, glycerol, and $(NH_4)_2SO_4$ are 75.14%, 49.82%, 34.26%, and 25.82%, respectively. The kinetics equation of catalytic reaction on these TNTAs photocatalysts has been studied by using first-order kinetics equation $\ln(C/C_0) = -kt$, in which k indicates the first kinetics equation constant. As shown in Figure 10(b), the catalytic rate constant in electrolyte of glycol, DMSO, glycerol, and $(NH_4)_2SO_4$ is 6.45×10^{-3}, 3.37×10^{-3}, 2.03×10^{-3}, and 1.42×10^{-3} min^{-1}, respectively. The order of catalytic rate constant is in accordance with the order of the length of nanotubes. For photocatalytic degradation on TiO_2 nanotube arrays, it is common sense that the amount of TiO_2 crystals will increase with increase of length of nanotube, which would exhibit better photocatalytic activity.

In order to further more effective composites by loading nanoparticles, however, those nanotubes prepared in electrolyte of glycol, DMSO shows their disadvantage of poor

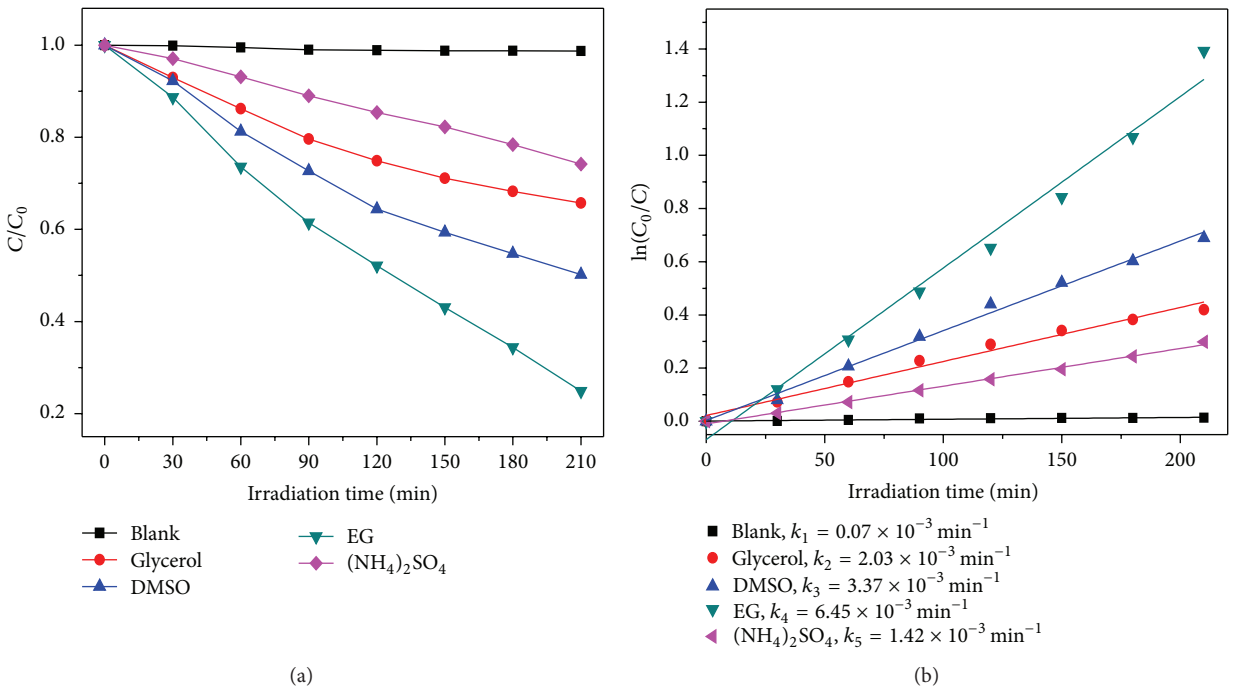

Figure 10: (a) Photocatalytic degradation of Rh B under UV light irradiation on various catalysts and (b) first-order kinetics data for the photodegradation of Rh B on various catalysts and the inset is the value of the rate constant k.

recycling efficiency. Firstly, the entrance of these tubes tends to collapse and snarls, which brings a great difficulty to decorate other nanoparticles on more widespread surface of TNTAs. Secondly, the overlong nanotubes increased the burden of Ti substrates, which makes nanotubes vulnerable and easier to fall off from substrates, when compared with other nanotubes having moderate length. And this will go against recycling and recovery of effective part of photocatalyst. To make composites by depositing nanoparticles on TNTAs, TNTAs prepared in glycerol under voltage of 20 V for 2 h are the best loading substrate, contributing by their uniform diameter, moderate length, and close adhesiveness with Ti foils.

4. Conclusions

The formation process of TNTAs strongly depends on the electrolytes. TNTAs formed in the electrolytes of glycol and DMSO grow along radial direction with flimsy tube wall and weak adhesion on Ti substrate. These TNTAs are not appropriate to assemble composite photocatalyst with other nanomaterials, although they show, respectively, higher catalytic activities. Those made in glycerol, however, easily achieve balance between growth rate and corrosion rate and form orderly arranged array of nanotubes with homogenous diameter, moderate length, and strong adhesiveness with substrates.

In addition, applied voltage and anodic oxidation duration crucially affect nanotube formation. Generally, longer time and higher voltage of oxidation will enhance length of nanotubes. However, the oxidation rate of Ti substrate and dissolve rate of nanotubes will be well balanced at condition of 20 V for 2 h. Consequently, TNTAs prepared in this condition will be the most appropriate loading substrates to further assemble functional composite nanomaterials.

Conflict of Interests

The authors declare that there is no conflict of interests regarding the publication of this paper.

Acknowledgments

This work is financially supported by the National Natural Science Foundation of China (NSFC Grant no. 21503146), International S&T Cooperation Program of China (no. 2013-DFG52490), The Training Program for Changjiang Scholars and Innovative Research Team in University ([2013]373), The Innovative Research Team of Tianjin Municipal Education Commission (TD125004), Scientific Research Foundation for the Introduction of Talent of Tianjin University of Science and Technology (no. 118510240), and Research Fund for the Doctoral Program of Higher Education of China (no. 20121208120001).

References

[1] M. Ye, D. Zheng, M. Lv, C. Chen, C. Lin, and Z. Lin, "Hierarchically structured nanotubes for highly efficient dye-sensitized solar cells," *Advanced Materials*, vol. 25, no. 22, pp. 3039–3044, 2013.

[2] S. Banerjee, S. K. Mohapatra, M. Misra, and I. B. Mishra, "The detection of improvised nonmilitary peroxide based explosives using a titania nanotube array sensor," *Nanotechnology*, vol. 20, no. 7, Article ID 075502, 2009.

[3] Y.-Y. Song and P. Schmuki, "Modulated TiO_2 nanotube stacks and their use in interference sensors," *Electrochemistry Communications*, vol. 12, no. 4, pp. 579–582, 2010.

[4] Y. Hou, X. Li, Q. Zhao, G. Chen, and C. L. Raston, "Role of hydroxyl radicals and mechanism of *Escherichia coli* inactivation on Ag/AgBr/TiO_2 nanotube array electrode under visible light irradiation," *Environmental Science and Technology*, vol. 46, no. 7, pp. 4042–4050, 2012.

[5] X. Wang, Y. Zhang, I. Baturin, and T. Liang, "Blocking effect of crystal-glass interface in lanthanum doped barium strontium titanate glass-ceramics," *Materials Research Bulletin*, vol. 48, no. 10, pp. 3817–3821, 2013.

[6] Q. Wang, J. Li, Y. Bai et al., "Photodegradation of textile dye Rhodamine B over a novel biopolymer-metal complex wool-Pd/CdS photocatalysts under visible light irradiation," *Journal of Photochemistry and Photobiology B: Biology*, vol. 126, pp. 47–54, 2013.

[7] W. Wilson, A. Manivannan, and V. R. Subramanian, "Heterogeneous photocatalytic degradation of recalcitrant pollutants over CdS—TiO_2 nanotubes: boosting effect of TiO_2 nanoparticles at nanotube—CdS interface," *Applied Catalysis A: General*, vol. 441-442, pp. 1–9, 2012.

[8] Q. Wang, X. Yang, D. Liu, and J. Zhao, "Fabrication, characterization and photocatalytic properties of Ag nanoparticles modified TiO_2NTs," *Electrochimica Acta*, vol. 83, p. 140, 2012.

[9] C. Chen, W. Ma, and J. Zhao, "Semiconductor-mediated photodegradation of pollutants under visible-light irradiation," *Chemical Society Reviews*, vol. 39, no. 11, pp. 4206–4219, 2010.

[10] X. Cheng, G. Pan, X. Yu, and T. Zheng, "Preparation of CdS NCs decorated TiO_2 nano-tubes arrays photoelectrode and its enhanced photoelectrocatalytic performance and mechanism," *Electrochimica Acta*, vol. 105, pp. 535–541, 2013.

[11] Y. Lai, J. Gong, and C. Lin, "Self-organized TiO_2 nanotube arrays with uniform platinum nanoparticles for highly efficient water splitting," *International Journal of Hydrogen Energy*, vol. 37, no. 8, pp. 6438–6446, 2012.

[12] Y. Yu, J. Ren, and M. Meng, "Photocatalytic hydrogen evolution on graphene quantum dots anchored TiO_2 nanotubes-array," *International Journal of Hydrogen Energy*, vol. 38, no. 28, pp. 12266–12272, 2013.

[13] J. Ran, J. Zhang, J. Yu, M. Jaroniec, and S. Z. Qiao, "Earth-abundant cocatalysts for semiconductor-based photocatalytic water splitting," *Chemical Society Reviews*, vol. 43, no. 22, pp. 7787–7812, 2014.

[14] P. Roy, S. Berger, and P. Schmuki, "TiO_2 nanotubes: synthesis and applications," *Angewandte Chemie—International Edition*, vol. 50, no. 13, pp. 2904–2939, 2011.

[15] M. Ni, M. K. H. Leung, D. Y. C. Leung, and K. Sumathy, "A review and recent developments in photocatalytic water-splitting using TiO_2 for hydrogen production," *Renewable and Sustainable Energy Reviews*, vol. 11, no. 3, pp. 401–425, 2007.

[16] X. Zhao, K. J. Aoki, J. Chen, and T. Nishiumi, "Examination of the Gouy-Chapman theory for double layer capacitance in deionized latex suspensions," *RSC Advances*, vol. 4, no. 108, pp. 63171–63181, 2014.

[17] D. Gong, C. A. Grimes, O. K. Varghese et al., "Titanium oxide nanotube arrays prepared by anodic oxidation," *Journal of Materials Research*, vol. 16, no. 12, pp. 3331–3334, 2001.

[18] S. Bauer, S. Kleber, and P. Schmuki, "TiO_2 nanotubes: tailoring the geometry in H_3PO_4/HF electrolytes," *Electrochemistry Communications*, vol. 8, no. 8, pp. 1321–1325, 2006.

[19] Y. Zhu, Z. Chen, T. Gao et al., "Construction of hybrid Z-scheme Pt/CdS-TNTAs with enhanced visible-light photocatalytic performance," *Applied Catalysis B: Environmental*, vol. 163, pp. 16–22, 2015.

[20] K. J. Aoki, X. Zhao, J. Chen, and T. Nishiumi, "Voltammetry in low concentration of electrolyte supported by ionic latex suspensions," *Journal of Electroanalytical Chemistry*, vol. 697, pp. 5–9, 2013.

[21] S. P. Albu, D. Kim, and P. Schmuki, "Growth of aligned TiO_2 bamboo-type nanotubes and highly ordered nanolace," *Angewandte Chemie—International Edition*, vol. 47, no. 10, pp. 1916–1919, 2008.

[22] J. M. Macak, H. Tsuchiya, A. Ghicov et al., "TiO_2 nanotubes: self-organized electrochemical formation, properties and applications," *Current Opinion in Solid State and Materials Science*, vol. 11, no. 1-2, pp. 3–18, 2007.

[23] J. M. Macak, H. Hildebrand, U. Marten-Jahns, and P. Schmuki, "Mechanistic aspects and growth of large diameter self-organized TiO_2 nanotubes," *Journal of Electroanalytical Chemistry*, vol. 621, no. 2, pp. 254–266, 2008.

[24] S. P. Albu, A. Ghicov, and P. Schmuki, "Erratum efficient solar energy conversion of TiO_2 nanotubes produced by rapid breakdown anodization—a comparison," *Rapid Research Letters (RRL)*, vol. 3, p. 64, 2009.

[25] Y.-Y. Song, R. Lynch, D. Kim, P. Roy, and P. Schmuki, "TiO_2 nanotubes: efficient suppression of top etching during anodic growth: key to improved high aspect ratio geometries," *Electrochemical and Solid-State Letters*, vol. 12, no. 7, pp. C17–C20, 2009.

[26] S. P. Albu and P. Schmuki, "Highly defined and ordered top-openings in TiO_2 nanotube arrays," *Physica Status Solidi (RRL)—Rapid Research Letters*, vol. 4, no. 7, pp. 151–153, 2010.

[27] J. Liao, S. Lin, L. Zhang, N. Pan, X. Cao, and J. Li, "Photocatalytic degradation of methyl orange using a TiO_2/Ti mesh electrode with 3D nanotube arrays," *ACS Applied Materials and Interfaces*, vol. 4, no. 1, pp. 171–177, 2012.

[28] X. Luan, D. Guan, and Y. Wang, "Facile synthesis and morphology control of bamboo-type TiO_2 nanotube arrays for high-efficiency dye-sensitized solar cells," *The Journal of Physical Chemistry C*, vol. 116, no. 27, pp. 14257–14263, 2012.

[29] X. Zhao, K. J. Aoki, J. Chen, and T. Nishiumi, "Which controls conductivity of sulfonic latex suspension, hydrogen ion or latex core?" *International Journal of Electrochemical Science*, vol. 9, no. 5, pp. 2649–2661, 2014.

[30] X. Zhang, F. Han, B. Shi, S. Farsinezhad, G. P. Dechaine, and K. Shankar, "Photocatalytic conversion of diluted CO_2 into light hydrocarbons using periodically modulated multiwalled nanotube arrays," *Angewandte Chemie—International Edition*, vol. 51, no. 51, pp. 12732–12735, 2012.

[31] H. Li, J.-W. Cheng, S. Shu et al., "Selective removal of the outer shells of anodic TiO_2 nanotubes," *Small*, vol. 9, no. 1, pp. 37–44, 2013.

[32] H. Cao, Z. Wang, G. Hou, and G. Zheng, "TiO_2 nanotube-supported amorphous Ni-B electrode for electrocatalytic oxidation of methanol," *Surface and Coatings Technology*, vol. 205, no. 3, pp. 885–889, 2010.

[33] Q. Kang, Q. Z. Lu, S. H. Liu et al., "A ternary hybrid CdS/Pt-TiO_2 nanotube structure for photoelectrocatalytic bactericidal effects on Escherichia Coli," *Biomaterials*, vol. 31, no. 12, pp. 3317–3326, 2010.

[34] Q. Z. Xu, X. Y. Wang, X. L. Dong, C. Ma, X. F. Zhang, and H. C. Ma, "Improved visible light photocatalytic activity for TiO_2 nanomaterials by codoping with zinc and sulfur," *Journal of Nanomaterials*, vol. 2015, Article ID 157383, 8 pages, 2015.

[35] W. Guan, F. Y. Ji, Z. G. Xie, R. A. Li, and N. Mei, "Preparation and photocatalytic performance of nano-TiO_2 codoped with iron III and lanthanum III," *Journal of Nanomaterials*, vol. 2015, Article ID 869821, 13 pages, 2015.

[36] M. Fujita, N. Idota, K. Matsukawa, and Y. Sugahara, "Preparation of oleyl phosphate-modified TiO_2/poly(methyl methacrylate) hybrid thin films for investigation of their optical properties," *Journal of Nanomaterials*, vol. 2015, Article ID 297197, 7 pages, 2015.

[37] D. Yu, B. Bo, and Y. He, "Fabrication of T iO_2@yeast-carbon hybrid composites with the raspberry-like structure and their synergistic adsorption-photocatalysis performance," *Journal of Nanomaterials*, vol. 2013, Article ID 851417, 8 pages, 2013.

[38] Q. Wang, J. Li, Y. Bai et al., "Photodegradation of textile dye Rhodamine B over a novel biopolymer-metal complex wool-Pd/CdS photocatalysts under visible light irradiation," *Journal of Photochemistry and Photobiology B: Biology*, vol. 126, pp. 47–54, 2013.